ACS APPLIED NANO MATERIALS

www.acsanm.org Article

Stable Infrared-Emitting Chemical Composition Gradient Quantum Dots for Down-Convertors and Photodetectors

Young Jun Yoon, Gill Biesold, Shuang Liang, Zewei Wang, Yeu Wei Harn, Cheng-Hsin Lu, Richard Kim, Wendy Yao, Sarah Lane, J. Christopher James, Yong Ding, Zhiqun Lin,* and Zhitao Kang*

Cite This: *ACS Appl. Nano Mater.* 2020, 3, 11335−11343 Read Online

ACCESS | Metrics & More | Article Recommendations | Supporting Information

ABSTRACT: Though remarkable breakthroughs have been made in visible-light-emitting quantum dots (QDs), the high potential in optoelectronic applications for efficient and stable infrared (IR)-emitting QDs has yet to be largely explored. The major obstacle for commercialization of these low-bandgap nanomaterials lies in their low chemical stability in ambient environments and difficulties in tuning and retaining the targeted optical characteristics. Herein, we report on a well-controlled yet facile cation-exchange strategy for crafting core/graded shell/shell QDs with precisely tailored spatial compositions to accurately regulate the optical properties in the IR region while simultaneously enhancing stability by utilizing CdSe/$Cd_{1-x}Zn_xSe_{1-y}S_y$/ZnS QD nanotemplates. PbSe/$PbSe_{1-y}S_y$/PbS QDs with tailored dimensions are yielded via a simple yet robust cation-exchange process that effectively replaces the Cd and Zn cations with the cation of interest (i.e., Pb) without disrupting the anionic framework. The absorption and emission of IR QDs can be precisely altered from 1200 to 2500 nm by either controlling the cation exchange time or tuning the dimensions and optical wavelengths of the inorganic nanotemplate (i.e., CdSe/$Cd_{1-x}Zn_xSe_{1-y}S_y$/ZnS QDs). These IR QDs manifest excellent colloidal stability in solution for months. Moreover, absorption wavelengths are well retained for more than 50 days without any noticeable shifts. Such a cation-exchange route is simple yet robust and may render the creation of a large variety of stable IR QDs of interest in a rapid and controllable manner for applications in IR-emitting down-converters, lasers, photodetectors, sensors, and so on.

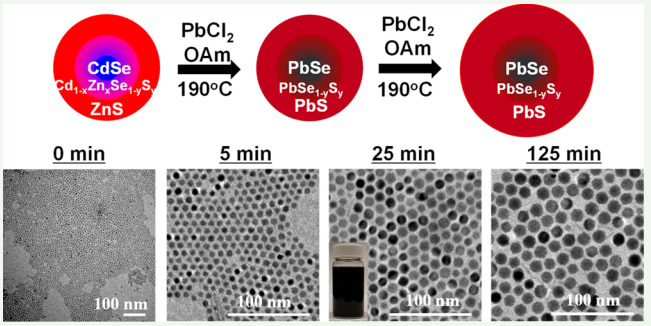

KEYWORDS: *quantum dots, nanoparticles, infrared emission, cation exchange, lead selenide, chemical composition gradient*

INTRODUCTION

Infrared (IR) semiconductor nanocrystals (NCs), so-called quantum dots (QDs), represent an important class of nanomaterials for next-generation optoelectronic applications such as lasing media, photodetectors, photoimaging devices, and IR scene projectors.[1,2] A variety of methods have been used to tune QD emission, including control of core size and shell thickness,[1] design of Type I or Type II QDs,[1] application of pressure,[3,4] and so on. To access photoluminescence (PL) and absorbance in the shortwave IR (SWIR; 1−2.5 μm) and midwave IR range (MWIR; 3−5 μm), materials with narrow bandgaps (<0.4 eV) are required. Among all narrow bandgap semiconductors, lead chalcogenide (i.e., PbS, PbSe, and PbTe) QDs have been widely studied. The exciton Bohr radii of PbS, PbSe, and PbTe are 18, 46, and 150 nm, respectively,[5] and the experimental values of direct energy bandgap for bulk PbS, PbSe, and PbTe at 300 K are 0.41, 0.27, and 0.31 eV, respectively.[6] Notably, PbSe has the narrowest bandgap among the three lead chalcogenides. In addition, PbSe is also known for its efficient multiple exciton generation (MEG) that may greatly improve light harvesting efficiency of solar cells as well as photodetectors.[7,8] The bandgap of these QDs can be fine-tuned by changing their sizes to below the respective Bohr radii, a phenomenon known as quantum confinement effect.[9−11] PbSe QDs, however, also have their own critical shortcomings, that is, low stability under ambient environments (e.g., susceptible to oxidation in air).[12−15] PbSe QDs dispersed in hexane and stored in air can undergo oxidation of up to 50% of its original volume in only a few hours.[15]

In this context, much effort has been centered on coating PbSe QDs with various materials to passivate the dangling Pb (e.g., $PbCl_2$[12] and PbS[16]) or Se (e.g., CdSe layer) sites on the QD surface, leading to their improved stability in ambient environments. Recently, a facile synthesis method was reported to produce stable PbSe QDs with a thin $PbCl_2$ outer coating

Received: September 7, 2020
Accepted: November 2, 2020
Published: November 11, 2020

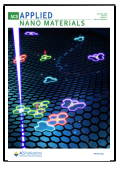

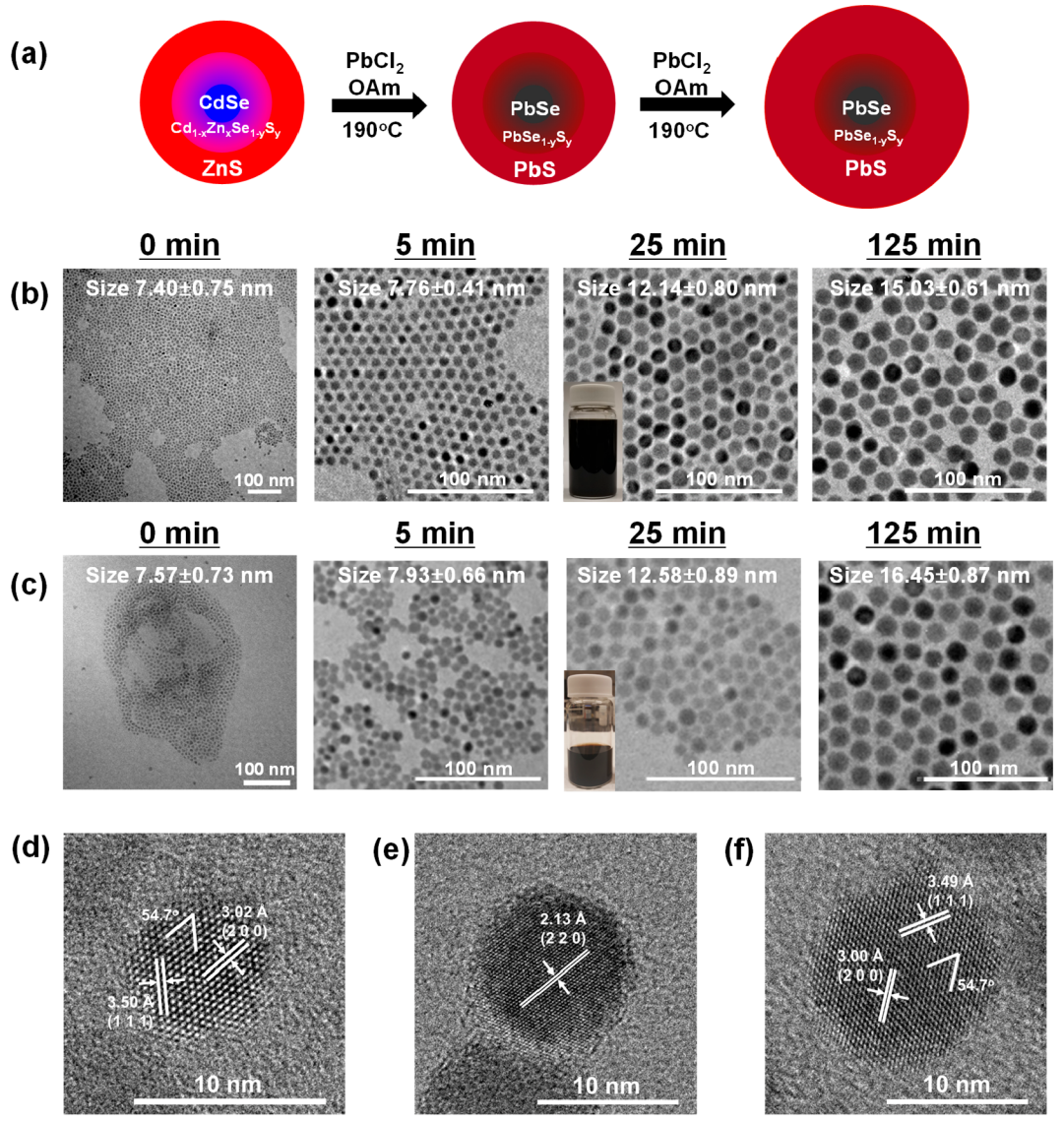

Figure 1. Cation exchange of CdSe/$Cd_{1-x}Zn_xSe_{1-y}S_y$/ZnS QDs into PbSe/$PbSe_{1-y}S_y$/PbS QDs. (a) Schematic representation of crafting PbSe/$PbSe_{1-y}S_y$/PbS QDs via cation exchange. TEM images of (b) PbSe/$PbSe_{1-y}S_y$/PbS QDs synthesized by utilizing green-emitting CdSe/$Cd_{1-x}Zn_xSe_{1-y}S_y$/ZnS QDs as nanotemplates and (c) PbSe/$PbSe_{1-y}S_y$/PbS QDs synthesized by employing red-emitting CdSe/$Cd_{1-x}Zn_xSe_{1-y}S_y$/ZnS QDs as nanotemplates. The left images in (b) and (c) are TEM images of the corresponding green- and red-emitting CdSe/$Cd_{1-x}Zn_xSe_{1-y}S_y$/ZnS QDs used as nanotemplates. (d–f) HRTEM images of PbSe/$PbSe_{1-y}S_y$/PbS QDs. (d) PbSe/$PbSe_{1-y}S_y$/PbS QDs cation-exchanged for 5 min from 7.40 nm green-emitting CdSe/$Cd_{1-x}Zn_xSe_{1-y}S_y$/ZnS QDs. (e) PbSe/$PbSe_{1-y}S_y$/PbS QDs cation-exchanged for 25 min from 7.40 nm green-emitting CdSe/$Cd_{1-x}Zn_xSe_{1-y}S_y$/ZnS QDs. (f) PbSe/$PbSe_{1-y}S_y$/PbS QDs cation-exchanged for 25 min from 7.57 nm red-emitting CdSe/$Cd_{1-x}Zn_xSe_{1-y}S_y$/ZnS QDs. The lattice spacing and crystalline planes are labeled in (d–f).

via cation exchange of CdSe[12] or ZnSe[17] QDs by utilizing $PbCl_2$ as the reactant. The cation exchange reaction was found to be effective. Moreover, by increasing the cation exchange time, the QD size continued to increase due to the Ostwald ripening effect even after the cation exchange process was complete.[18] Moreover, the initial cation exchange was instantaneous; however, the following growth phase was proceeded over minutes or even hours, thus rendering precise control over dimensions.

It is notable that in the case of PbSe/PbS core/shell QDs they possess a Type II core/shell structure (i.e., E_c(PbS) > E_c(PbSe) > E_v(PbS) > E_v(PbSe), where E_c and E_v are conduction band and valence band energies, respectively);[19] the spread of the hole wave function across the PbSe and PbS materials may thus occur, resulting in a red-shift in PL emission (relative to that of the PbSe core) and an extended exciton lifetime.[2,20] Moreover, thick shell layers are known to cause suppressed absorption intensity of the first exciton peak and induce a larger Stokes shift in QDs. In this regard, CdSe/$Cd_{1-x}Zn_xSe_{1-y}S_y$/ZnS core/graded shell/shell QDs synthesized by us have a gradient interface layer between CdSe and ZnS.[21] They exhibit suppressed absorption of the first-exciton peak and improved stability due to the reduced lattice mismatch between the core and shell materials.[21] It has been demonstrated that even for PbSe/PbS core/shell QDs with a small lattice mismatch of 3%, the alloying of the interface via thermal annealing have shown to reduce interfacial strain, leading to longer PL lifetimes.[22] In addition, quantum yield (QY) of PbSe/$PbSe_{1-y}S_y$ (y = 0.5) core/alloyed shell QDs was reported to be 65% compared to 40% of PbSe core only QDs

https://dx.doi.org/10.1021/acsanm.0c02434
ACS Appl. Nano Mater. 2020, 3, 11335−11343

and 50% of PbSe/PbS core/shell QDs.[20] It is worth noting that suppressed first exciton peak absorption, PL red-shift, and high QY are of key importance, especially for PbSe-based QDs which show anti-Stokes shift as the size of plain PbSe QD increases. For instance, 4 nm PbSe QDs have a Stokes shift of 100 meV while that of 6.1 nm PbSe QDs is −10 meV.[20]

Herein, we develop a robust route to stable IR-emitting chemical composition gradient QDs (i.e., PbSe/PbSe$_{1-y}$S$_y$/PbS core/graded shell/shell QDs) with precisely tunable dimensions and optical properties by controlling the cation-exchange (CE) reaction time as well as the dimensions of initial inorganic nanotemplate (i.e., CdSe/Cd$_{1-x}$Zn$_x$Se$_{1-y}$S$_y$/ZnS QDs). The CE reaction involves an instantaneous CE reaction, followed by slow growth of the PbS shell layer which is simply attainable by extending the CE time. Such a reaction not only improves the stability of the resulting QDs but also allows for fine-tuning of their emission wavelengths. Furthermore, by first synthesizing a more readily characterizable CdSe/Cd$_{1-x}$Zn$_x$Se$_{1-y}$S$_y$/ZnS QDs (i.e., CdSe and ZnS having distinct lattice dimensions as well as optical properties in the visible region) of different sizes and subsequently performing CE to craft PbSe/PbSe$_{1-y}$S$_y$/PbS QDs of varied diameters, the relationship between the crystal dimensions and optical properties is scrutinized. It is important to note that the PbSe core is directly surrounded by a PbS shell in situ, thus preventing the PbSe core from being exposed to air and in turn ensuring improved stability. They demonstrate outstanding colloidal stability for months, and the absorption wavelengths remain unchanged for more than 50 days. As such, stable IR-emitting QDs of varied dimensions are easily accessible. By extension, a rich diversity of SWIR and MWIR QDs of interest with long-term stability can be conveniently produced by the facile CE strategy, rendering a wide range of optoelectronic applications.

RESULTS AND DISCUSSION

Figure S1a depicts the schematic representation of CdSe/Cd$_{1-x}$Zn$_x$Se$_{1-y}$S$_y$/ZnS QDs with a composition gradient interface between the CdSe core and ZnS shell as well as a thicker passivating ZnS shell layer (right column). The synthesis details are given in the Experimental Section as well as our previous work.[21] The gradient interface between the core and shell material allows for the delocalization of electrons into the interfacial layer, thus rendering a red-shift in the optical properties compared to the CdSe core only while concurrently reducing the strain and instability caused by the lattice mismatch between the CdSe core and ZnS shell. This composition gradient interface is achieved by capitalizing on the higher reactivity between Cd and Se compared to that between Zn and Se, thus imparting more Cd to occupy the inner core and more Zn to take up the outer shell. The thick ZnS shell is achieved by adding excess Zn and S compared to Cd and Se. Figure S1a (left column) and Figure S1b show the absorption and emission spectra and TEM images of the chemical composition gradient QDs, respectively, prepared by using 2.45 nm green-emitting CdSe QDs as the seeds. The diameter of QDs increased from 2.45 nm for as-prepared CdSe QD core (i.e., 2.45 nm calculated from the first exciton peak wavelength[23]) to 5.25 nm for CdSe/Cd$_{1-x}$Zn$_x$Se$_{1-y}$S$_y$/ZnS QDs with a thin ZnS outer shell and 7.40 nm for CdSe/Cd$_{1-x}$Zn$_x$Se$_{1-y}$S$_y$/ZnS QDs with a thick ZnS outer shell. Notably, because of the suppressed absorption peak, it is unclear where the absorption peak is exactly situated for the CdSe/Cd$_{1-x}$Zn$_x$Se$_{1-y}$S$_y$/ZnS QDs. However, from the PL peak position shift of 13 nm, a 6.5% increase of the effective core diameter can be estimated due to the gradient interface between the core and shell materials. As one monolayer of ZnS is 3.1 Å, the 5.25 nm CdSe/Cd$_{1-x}$Zn$_x$Se$_{1-y}$S$_y$/ZnS QDs have 4.3 ZnS layers, while the 7.40 nm CdSe/Cd$_{1-x}$Zn$_x$Se$_{1-y}$S$_y$/ZnS QDs possess 7.7 ZnS layers (a monolayer of ZnS is 3.1 Å between consecutive planes along the [002] axis in bulk wurtzite ZnS[24]). Figure S2 displays the absorption and emission spectra of three CdSe/Cd$_{1-x}$Zn$_x$Se$_{1-y}$S$_y$/ZnS QDs, each emitting a red, green, and blue color (hereafter denoted Red, Green, and Blue QDs). All three QDs are synthesized by utilizing the chemical reactivity differences between the reactants to yield a gradient interface (see the Experimental Section).

Figure 1a depicts the synthetic scheme for converting the highly stable CdSe/Cd$_{1-x}$Zn$_x$Se$_{1-y}$S$_y$/ZnS QDs to PbSe/PbSe$_{1-y}$S$_y$/PbS QDs in a one-step CE reaction. The CE process is driven by the difference in solvation energy for the cations (i.e., the ligand's propensity for selective ion binding).[18,25,26] Previous studies have demonstrated that both Zn and Cd can readily be replaced with Pb.[2] Oleylamine, in particular, has been shown to be critical to solvate Cd ions and allow for replacement with Pb. Cation exchange with Pb oleate alone has not resulted in any successful substitution. In both this study and previous ones, Pb substitution has been observed to occur rapidly, needing only 20 s in some cases. It is worth noting that after initial CE the PbS shell thickness continues to grow, and this process is finely tunable by simply changing the reaction time. This process is a result of the Ostwald ripening effect, where smaller particles dissolve and redeposit on larger particles. The ability to precisely control the PbS shell thickness over a PbSe core is important as PbSe/PbSe$_{1-y}$S$_y$/PbS QDs are Type II core/shell QDs in which the alignment of the bandgap may confer emission to red-shift as a function of the shell thickness. The schematics of Type II band alignment of PbSe/PbS and gradient PbSe/PbSe$_{1-y}$PbS$_y$/PbS QDs are shown in Figure S3. For comparison, the schematics of Type I band alignment of CdSe/ZnS and CdSe/Cd$_{1-x}$Zn$_x$Se$_{1-y}$S$_y$/ZnS QDs are shown in Figure S4.

Figures 1b,c show TEM images of the chemical composition gradient PbSe/PbSe$_{1-y}$S$_y$/PbS QDs produced by utilizing CdSe/Cd$_{1-x}$Zn$_x$Se$_{1-y}$S$_y$/ZnS QDs (Figure 1b: CE from 7.40 nm Green QDs in Figure S2; Figure 1c: CE from 7.57 nm Red QDs in Figure S2) as nanotemplates. The TEM images clearly reveal that both QDs before and after CE are monodisperse. One simple and direct indication of CE can be seen from the inset (i.e., digital image of the colloidal solution in Figure 1c), in which the normally green or red cadmium-based QDs are fully converted to a dark-brown color, indicative of lead-based QDs. Moreover, from the inset, we note that the lead-based QD is colloidally stable in solution. Even after over one year of storage in air at RT, we did not observe any precipitation. The diameter of the QDs increases from 7.40 ± 0.75 nm for as-prepared CdSe/Cd$_{1-x}$Zn$_x$Se$_{1-y}$S$_y$/ZnS QDs (Green QDs; Figure 1b) to 7.76 ± 0.41 nm for the PbSe/PbSe$_{1-y}$S$_y$/PbS QDs cation-exchanged for 5 min, to 12.14 ± 0.80 nm for the PbSe/PbSe$_{1-y}$S$_y$/PbS QDs cation-exchanged for 25 min, and eventually to 15.03 ± 0.61 nm for the PbSe/PbSe$_{1-y}$S$_y$/PbS QDs cation-exchanged for 125 min. Considering the near-complete CE that is further corroborated in the later sections, the density of the components (Table S1), and PbS monolayer thickness of 1.2 nm,[27] there is approximately 4.3, 7.9, and 10.3

https://dx.doi.org/10.1021/acsanm.0c02434
ACS Appl. Nano Mater. 2020, 3, 11335−11343

PbS layers after 5, 25, and 125 min, respectively. As the 7.40 nm CdSe/$Cd_{1-x}Zn_xSe_{1-y}S_y$/ZnS QD nanotemplate has 7.7 ZnS layers, the initial drop to 4.3 PbS layers coincides with our proposed schematic in Figure 2b and prior literature[17] in which

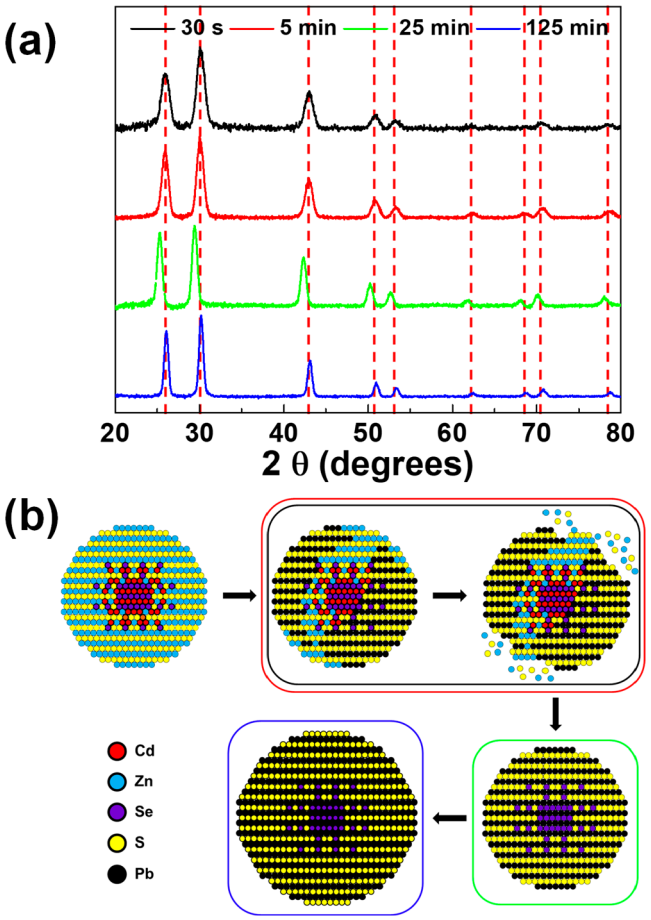

Figure 2. Cation-exchange mechanism of CdSe/$Cd_{1-x}Zn_xSe_{1-y}S_y$/ZnS QDs into PbSe/$PbSe_{1-y}S_y$/PbS QDs as substantiated by XRD. (a) XRD of PbSe/$PbSe_{1-y}S_y$/PbS QDs after different cation exchange times (30 s, 5 min, 25 min, and 125 min) from 7.57 nm red-emitting CdSe/$Cd_{1-x}Zn_xSe_{1-y}S_y$/ZnS QDs. (b) Schematic showing the possible cation-exchange mechanism based on XRD data. The XRD data and schematic are color-coded.

the shell layer is partially lost for large quantum dots initially and then later replenished as the cation exchange reaction progresses. The 7.57 ± 0.73 nm red-emitting CdSe/$Cd_{1-x}Zn_xSe_{1-y}S_y$/ZnS QDs also exhibit a very similar trend where the size increase is precisely controllable as a function of CE time. Figure 1d–f and Figure S5 show HRTEM images of PbSe/$PbSe_{1-y}S_y$/PbS QDs with excellent crystallinity. Because of the small crystallographic mismatch between PbSe and PbS of 3%,[20] the QDs appear to be a single crystal. The lattice spacing, however, show values that are intermediate of the characteristic values for PbSe (#78-1903) and PbS (#78-1900). For instance, PbSe/$PbSe_{1-y}S_y$/PbS QDs (Green QD cation-exchanged for 5 min; Figure 1d) and PbSe/$PbSe_{1-y}S_y$/PbS QDs (Red QD cation-exchanged for 25 min; Figure 1f) have a lattice spacing of 0.350 nm (111) and 0.349 nm (111), respectively, that is in between that of 0.353 nm for PbSe and that of 0.342 nm for PbS. This observation also agrees well with the intermediate XRD peaks that will be discussed later.

We note that the QD size increases via two distinct processes. First, the crystal density of the reactant QD is much lower than that of the product QD (Table S1). Although the volumetric change in the core material from CdSe to PbSe is relatively small (4.5% increase from zinc-blende CdSe or 7.5% increase from wurtzite CdSe), the volumetric change in the shell material from ZnS to PbS is significant (32.1% increase from zinc-blende ZnS). Second, it has been reported that the materials to grow larger QDs are provided via the Ostwald ripening effect in which smaller QDs dissolve and redeposit on larger QDs. One limitation of the CE of core/shell QDs may be that it is not clear when the core material (Se) will dissolve and deposit on the PbSe/$PbSe_{1-y}S_y$/PbS QD shell. The amount of Se, however, compared to S in the reactant is very small (molar ratio 1:45). To substantiate this, XPS was used to show that a detectable amount of Se is not present on the surface of the PbSe/$PbSe_{1-y}S_y$/PbS QDs (Figure S6).

Figure S7 shows the suppressed absorption spectra of PbSe/$PbSe_{1-y}S_y$/PbS QDs due to the thick outer PbS shell. The first exciton absorption peak is completely unobservable when viewed over the entire spectrum. A close-up shown in Figure S7b reveals the presence of a weak first exciton absorption peak at ∼1800 nm. As the PbSe/$PbSe_{1-y}S_y$/PbS QD size increases from 7.76 nm (Green QDs cation exchanged for 5 min) to 12.14 nm (Green QDs cation exchanged for 25 min), however, this absorption peak is clearly suppressed due to the absorption primarily from the thick PbS shell. It is notable that the suppression of the first exciton absorption peak was not seen for PbSe/$PbSe_{1-y}S_y$ QDs (i.e., synthesized via CE of CdSe/$Cd_{1-x}Zn_xSe_{1-y}S_y$ QDs without a ZnS shell; see the Experimental Section) that did not possess a PbS shell (Figure S8).

Figure 2b depicts the proposed CE mechanism of the Red CdSe/$Cd_{1-x}Zn_xSe_{1-y}S_y$/ZnS QDs to PbSe/$PbSe_{1-y}S_y$/PbS QDs via XRD analysis (Figure 2a). The XRD profiles and schematic are color-coded to match each other. Figure S9 shows the XRD peak positions of the PbSe/$PbSe_{1-y}S_y$/PbS QD relative to those for PbSe, PbS, CdSe, and ZnS. After just 30 s of CE, the characteristic peaks for the CdSe/$Cd_{1-x}Zn_xSe_{1-y}S_y$/ZnS QDs completely disappear (XRD of the Red QDs is shown in Figure S10), and only those for either PbSe or PbS are observed based on the XRD analysis. The XRD peaks overlap more precisely with that of PbS (#78-1900) in the earlier stages of CE (i.e., CE for 30 s and 5 min). As shown in Figure 2 (black and red box), it is likely that the CE process initiates from the outer shell material, creating an overwhelming signal from the outer PbS shell material compared to that of the PbSe core material. As the CE process advances toward the inner core (i.e., CE for 25 min), the XRD peaks shift more toward that of the PbSe (#78-1903) material, thus positioning themselves intermediate between that of the PbSe and PbS. It is hypothesized that the XRD peaks shift toward PbSe due to the gradual construction and crystallization of rock-salt PbSe phase from the residual Cd-containing intermediate Pb(Cd)Se phase in the inner core. Similar observations have been previously reported in the literature where alloy structures of two compounds show intermediate XRD peaks.[28] As PbSe/$PbSe_{1-y}S_y$/PbS QDs also carry an interfacial gradient layer, where there is a mixture of PbSe and PbS materials, the intermediate XRD peak position supports the successful synthesis of PbSe/$PbSe_{1-y}S_y$/PbS QDs with an interfacial composition gradient. As the reaction continues to 125 min, the characteristic peaks shift back to

https://dx.doi.org/10.1021/acsanm.0c02434
ACS Appl. Nano Mater. 2020, 3, 11335−11343

higher angles, which overlap more with those of the PbS (#78-1900) peaks. This is because, as the CE process progresses, a thicker PbS shell is formed on the outside of PbSe/PbSe$_{1-y}$S$_y$/PbS QDs; so the overwhelming signal from the PbS material dominates. It is worth noting that we also performed the same measurements for the PbSe/PbSe$_{1-y}$S$_y$/PbS QDs cation-exchanged from the Green QDs (Figures S11−S13). The results demonstrate a similar trend to that observed in Figure 2. However, the shift to lower angles (XRD peaks for PbSe are situated at lower angles compared to PbS) after 25 min is less pronounced (Figure S14), which strongly corroborates the proposed CE mechanism. In other words, for the Green QDs there is less Se compared to that in the Red QDs; thus, there will be less PbSe in the final cation-exchanged QDs as well, resulting in a less pronounced shift toward lower angles where the characteristic peaks of PbSe is situated. To further verify complete CE from Cd and Zn into Pb, the PL of the PbSe/PbSe$_{1-y}$S$_y$/PbS QD solution was measured along the visible wavelengths. Figure S15a compares the PL of the Red-emitting QDs and the corresponding PbSe/PbSe$_{1-y}$S$_y$/PbS QDs (Red QD cation-exchanged for 30 s). After only 30 s of CE, PL across the visible spectrum completely disappeared. Even if the PbSe/PbSe$_{1-y}$S$_y$/PbS QD PL curve in Figure S15a is magnified, there is no small bump that may indicate PL emission. We then moved to test the device limits by measuring even the weakest PL from the QDs while exciting the QDs with the strongest excitation possible from the spectrophotometer (excitation slit width 15 nm; emission slit width 20 nm; sensitivity set to high). This setting would not be used in normal circumstances as even QDs with extremely low QY (e.g., <1%) will show PL counts over the detection limit. Under these extreme settings, we were able to observe a small PL peak from residual CdSe in the PbSe/PbSe$_{1-y}$S$_y$/PbS QDs cation-exchanged for 30 s and 5 min (Figure S15b). The small PL peak, however, completely disappeared for PbSe/PbSe$_{1-y}$S$_y$/PbS QDs cation-exchanged for 25 min, further substantiating our proposed mechanism in Figure 2b in which complete cation exchange takes place by 25 min.

As complete CE occurred between the CE reaction time of 5 and 25 min, energy-dispersive X-ray spectroscopy (EDS; Figures S16 and S17) was performed to further verify the elemental composition of the PbSe/PbSe$_{1-y}$S$_y$/PbS QDs cation-exchanged for 5 and 25 min. Figure S16 shows point-scan of EDS measurements performed via HRTEM, and Figure S17 shows area-scan of EDS measurements performed via SEM. Although overlap of the peaks for several atom types prevents us from clearly determining the quantitative presence of each element, it is evident that the Pb signals overwhelm that of either Cd or Zn atoms. The peak, assigned to Cu and Zn in Figure S16, is likely originated from only Cu, as the signal at that position disappeared in Figure S17 where the sample holder does not contain a copper grid while that for the HRTEM does include the copper grid. Moreover, fluorescence lines assigned to the K transition of Zn (Ka1 8637 eV; Ka2 8614 eV; Ka3 8463 eV) is completely absent in Figure S16 as well, further corroborating the complete removal of Zn. As for Cd (La1 3133 eV; Lb1 3315 eV), there is also no clear signal observed in Figure S16 or S17. It seems EDS measurements are not sensitive enough to distinguish the difference between the PbSe/PbSe$_{1-y}$S$_y$/PbS QDs cation-exchanged for 5 and 25 min. However, they do further validate the successful CE reaction and the negligible presence of Cd and Zn atoms in the QDs.

To further corroborate that the original anionic framework is retained during cation exchange, we performed EDS mapping via HRTEM. Figure S18a shows the HRTEM of PbSe/PbSe$_{1-y}$S$_y$/PbS QDs (Red QD cation-exchanged for 5 min) with excellent crystallinity in bright field and dark field. Figure S18b shows the EDS mapping of a single QD from the same sample. It is important to emphasize that S could not be mapped via EDS as the S signal overlaps with that of Pb. We thus show the elemental map via EDS for Pb and Se. As the original CdSe/Cd$_{1-x}$Zn$_x$Se$_{1-y}$S$_y$/ZnS QDs were made by a modified version of previously reported composition gradient QDs,[21,34] the elemental map in Figure S18b, in which there is relatively more Se in the center region with a gradual decline toward the edges and a more even distribution of Pb throughout the QD, further corroborates that the original structure is retained after the cation exchange process. Moreover, we would like to emphasize that in Figure 16c the point scan EDS in the center of the PbSe/PbSe$_{1-y}$S$_y$/PbS QDs (Red QD cation-exchanged for 25 min) has a stronger Se signal (Ka1 11224 eV; Ka2 11183 eV) compared to that in PbSe/PbSe$_{1-y}$S$_y$/PbS QDs (Green QD cation-exchanged for 25 min). This observation further corroborates that the original CdSe/Cd$_{1-x}$Zn$_x$Se$_{1-y}$S$_y$/ZnS QD morphology of the template is maintained after cation exchange.

Figure 3 shows the stability of PbSe/PbSe$_{1-y}$S$_y$/PbS QDs by measuring the absorption peak position after storage under

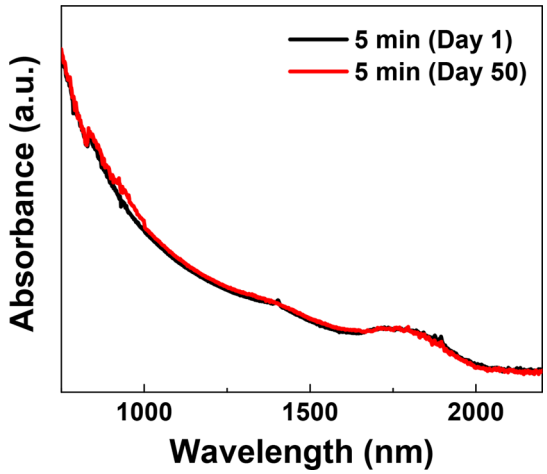

Figure 3. Stability of PbSe/PbSe$_{1-y}$S$_y$/PbS QDs evidenced by no absorption peak shift. The PbSe/PbSe$_{1-y}$S$_y$/PbS QDs are dispersed in tetrachloroethylene and exposed to ambient air and light. PbSe/PbSe$_{1-y}$S$_y$/PbS QDs (Green QD cation-exchanged for 5 min) are exploited, as QDs with thicker shells have stronger absorption suppression, making it difficult to decipher the first exciton peak position.

ambient environment (dispersed in tetrachloroethylene and exposed to light and air at room temperature) for 50 days. It has been reported that PbSe QDs which are easily oxidized when exposed to air would show a blue-shift in the absorption peak in less than a week.[15] In stark contrast, PbSe/PbSe$_{1-y}$S$_y$/PbS QDs show no noticeable shift in the absorption peak position after 50 days. All PbSe/PbSe$_{1-y}$S$_y$/PbS QD batches synthesized manifest no shift in the peak position; however, it is relatively difficult to discern for QDs with a thicker PbS shell (i.e., CE for 25 min) due to suppressed absorption as shown in Figure S7b. We attribute the enhanced stability to the thick PbS shell. PbS QDs have been demonstrated to be both water

https://dx.doi.org/10.1021/acsanm.0c02434
ACS Appl. Nano Mater. 2020, 3, 11335−11343

and air stable for over several months.[29,30] In addition, chlorine surface passivation, a possible cause for the stability enhancement, was verified via XPS as shown in Figure S19.

Figure 4a presents the PL of PbSe/PbSe$_{1-y}$S$_y$/PbS QDs after different CE times. Obviously, PbSe/PbSe$_{1-y}$S$_y$/PbS QDs with

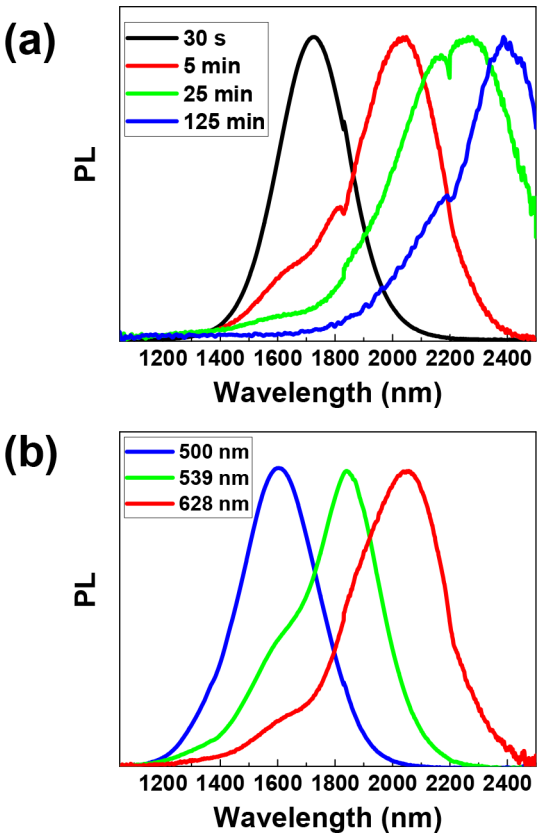

Figure 4. PL of PbSe/PbSe$_{1-y}$S$_y$/PbS QDs after cation exchange. (a) Effect of cation exchange time on final PL. The four PbSe/PbSe$_{1-y}$S$_y$/PbS QDs are synthesized via cation exchange of red-emitting CdSe/Cd$_{1-x}$Zn$_x$Se$_{1-y}$S$_y$/ZnS QDs as nanotemplates. (b) Effect of CdSe/Cd$_{1-x}$Zn$_x$Se$_{1-y}$S$_y$/ZnS QD nanotemplate dimensions on final PL. The three PbSe/PbSe$_{1-y}$S$_y$/PbS QDs are cation-exchanged for 5 min. All samples are dispersed in tetrachloroethylene to minimize IR absorption by solvent.

IR emission have been successfully synthesized. It is interesting to note that there is a constant red-shift in the PL emission as the CE reaction progresses due to the Type II QD structure. This result is in good agreement with previous studies which have demonstrated that core−shell PbSe/PbS and PbSe/PbSe$_x$S$_{1-x}$ QDs exhibit red-shifted emission with increasing shell size.[27] After a 125 min CE reaction, the PL is at ∼2400 nm, which is a distinct shift from ∼1700 nm (CE for 30 s) or ∼2050 nm (CE for 5 min). It is noteworthy that for a PbSe core-only QD a 2400 nm PL peak would correspond to ∼9.3 nm.[10] From the absorption data of the Red QDs in Figure S2, the effective core size (i.e., size of the CdSe/Cd$_{1-x}$Zn$_x$Se$_{1-y}$S$_y$) is calculated to be ∼5.3 nm. Even considering the size increase of the effective core after CE due to the increase in the molar volume, the effective core size cannot increase to 9.3 nm, which would be a 75% increase. Thus, the PL extension to 2400 nm is unambiguously influenced by the PbS shell layer. As for the broad shoulder at low wavelengths (1400−1800 nm) seen for the PbSe/PbSe$_{1-y}$S$_y$/PbS QDs cation-exchanged for 5 min, it is due likely to QDs that have not been fully cation-exchanged. This is corroborated by the PL peak for the PbSe/PbSe$_{1-y}$S$_y$/PbS QDs cation-exchanged for 125 min (i.e., a complete CE) where no shoulder peak is observed.

The photoluminescence quantum yield (PLQY) (η) of four representative samples with emissions ranging from 1600 to 2400 nm was measured by using a method similar to that reported in the literature[31] (full details in the Experimental Section). The obtained PLQY values are shown in Table 1.

Table 1. Measured PLQY of PbSe/PbSe$_{1-y}$S$_y$/PbS QDs Ranging from 1600 to 2400 nm

emitted wavelength [nm]	PLQY [%]
1600	41
1800	23
2000	16
2400	3

The decrease in PLQY as a function of increasing emitted wavelength is commonly reported and is attributed to nonradiative exciton relaxation facilitated by strong electronic coupling between QDs and organic ligand layers through both direction wave function mixing and energy transfer.[10] The PLQY values of the CE-derived PbSe QDs are somewhat lower than other reported values for PbSe QDs,[10] though the values are comparable. The discrepancy in PLQY values could arise from the testing errors resulted from the very low PLQY (∼0.1%) of the available IR dye reference.

In addition to the CE reaction time that dictates the optical properties (i.e., absorption and PL) of PbSe/PbSe$_{1-y}$S$_y$/PbS QDs (Figure 4a), the starting CdSe/Cd$_{1-x}$Zn$_x$Se$_{1-y}$S$_y$/ZnS QD emission wavelength (or size) also influences the optical properties of PbSe/PbSe$_{1-y}$S$_y$/PbS QDs after identical CE times (Figure 4b). Figure 4b shows the PL of three PbSe/PbSe$_{1-y}$S$_y$/PbS QDs synthesized by utilizing the Red, Green, and Blue CdSe/Cd$_{1-x}$Zn$_x$Se$_{1-y}$S$_y$/ZnS QDs, respectively, as nanotemplates. All three CE reactions are performed for 5 min. It is clear that the change in optical properties of CdSe/Cd$_{1-x}$Zn$_x$Se$_{1-y}$S$_y$/ZnS QDs via control over the QD dimensions is directly translated into the tailoring of optical properties of the resulting PbSe/PbSe$_{1-y}$S$_y$/PbS QDs. The PbSe/PbSe$_{1-y}$S$_y$/PbS QDs synthesized from the Red QDs (emission wavelength; λ_{em} = 628 nm) emit at ∼2057 nm, while those synthesized from QDs with a smaller core (Green QDs, λ_{em} = 539 nm; Blue QDs, λ_{em} = 500 nm) emit at 1839 and 1604 nm, respectively. This is because the CE process simply replaces the Cd and Zn cations with Pb cations from the more sturdy Se and S anionic framework. To demonstrate the potential use of PbSe/PbSe$_{1-y}$S$_y$/PbS QDs as down-converters in IR-emitting light sources similar to phosphor-converted LEDs,[32] IR QD LEDs were successfully fabricated by coating PbSe/PbSe$_{1-y}$S$_y$/PbS QDs on top of a GaN blue LED chip, and the corresponding IR PLs are shown in Figure S20. However, the QD coatings prepared with polymer solutions were too thin to absorb most of the blue LED emission. In-situ polymerization of the QD−monomer solution on LED chips to form thick uniform coatings is under investigation to increase blue light absorption and reduce IR light reabsorption between QDs. In addition, these IR-emitting QDs also hold promising applications in lasers, photodetectors, and sensors.

https://dx.doi.org/10.1021/acsanm.0c02434
ACS Appl. Nano Mater. 2020, 3, 11335−11343

CONCLUSION

In summary, we demonstrated the precision synthesis of composition gradient PbSe/$PbSe_{1-y}S_y$/PbS IR QDs by capitalizing on CE of well-defined presynthesized CdSe/$Cd_{1-x}Zn_xSe_{1-y}S_y$/ZnS visible QDs as nanotemplates, thereby rendering a robust tailoring of the optical properties in the IR region and concurrently enhancing their stability. The chemical composition gradient CdSe/$Cd_{1-x}Zn_xSe_{1-y}S_y$/ZnS QD nanotemplates are first synthesized by exploiting well-known chemical reactivity differences between the reactants. The CE reaction, in which the sturdy anion framework is retained while selectively replacing the cations, is successfully conducted. Specifically, the selective substitution of Cd and Zn atoms with Pb atoms was enabled by creating a solution environment where the selected ligand binding with Cd and Zn atoms is more favorable that that with Pb atoms. Because of the difference in crystal density between the reactant CdSe/$Cd_{1-x}Zn_xSe_{1-y}S_y$/ZnS QDs and product PbSe/$PbSe_{1-y}S_y$/PbS QDs, the size of the QDs increase after the CE reaction. Moreover, by utilizing Ostwald ripening effect, the PbS shell layer on the PbSe/$PbSe_{1-y}S_y$/PbS QDs is precisely tunable as a function of CE time and reproducible as the PbS shell growth takes place over minutes and not seconds. The crafted PbSe/$PbSe_{1-y}S_y$/PbS QDs carry a broad PL range between 1200 and 2500 nm (SWIR region) as a function of CE time. It is important to note that not only the CE time but also the initial CdSe/$Cd_{1-x}Zn_xSe_{1-y}S_y$/ZnS QD size exerted a profound influence on the absorption and emission of PbSe/$PbSe_{1-y}S_y$/PbS QDs in the IR region. Clearly, the prolonged CE reaction time as well as the use of even larger-sized starting CdSe/$Cd_{1-x}Zn_xSe_{1-y}S_y$/ZnS QDs would extend the absorbance and PL of the resulting PbSe/$PbSe_{1-y}S_y$/PbS QDs to MWIR ranges (>3000 nm). Finally, to produce environmentally benign MWIR QDs, CE reactions by utilizing Ag atoms may also be conducted as well.[33] This will be the subject of future work. Nonetheless, the CE strategy provides a simple yet powerful platform for devising a rich array of stable IR QDs for use in optoelectronic materials and devices.

EXPERIMENTAL SECTION

Materials. Lead(II) chloride ($PbCl_2$) (ultradry, 99.999%), selenium powder (200 mesh, 99.999%), sulfur powder (precipitated, 99.5%), cadmium oxide (98.9%), zinc acetate dihydrate ($ZnAc_2$) (ACS reagent grade, 98.0−101.0%), trioctylphosphine oxide (TOPO) (>98%), 1-octadecene (ODE) (tech. grade, 90%), oleic acid (OA) (tech. grade, 90%), and tetrachloroethylene (TCE) (ultrapure, spectrophotometric grade, 99+%) were obtained from Alfa Aesar. Trioctylphosphine (TOP) (97%), octadecylphosphonic acid (ODPA) (97%), zinc acetylacetonate hydrate, and 1-dodecanethiol (>98%) were obtained from Sigma-Aldrich. Oleylamine (OAm) (50.0%) was obtained from TCI Chemicals. Toluene, hexane, and methanol (ACS reagent grade) were obtained from BDH Chemicals. All chemicals were used as received without any further purification.

Synthesis of CdSe QD Core. ODPA-capped CdSe QDs were synthesized by following a reported method.[33] A mixture of CdO (50 mg), ODPA (400 mg), and TOPO (4 g) was placed in a three-neck flask and degassed at 140 °C for 1 h. The temperature was then raised to 290 °C. After complete solubilization of the reactants that the solution became transparent and colorless, 1 mL of 1 M Se/TOP solution was quickly injected into the reaction flask to initiate nucleation and growth. The heating mantle was removed, and the reaction flask was quickly placed in a water bath. Five milliliters of toluene was added as the reaction solution reached 60 °C. The resulting ODPA-capped CdSe QDs were precipitated with methanol twice and dispersed in toluene.

Preparation of Cd-Oleate and Zn-Oleate Precursor Solution. We placed 154 mg of CdO, 1581 mg of zinc acetyl acetonate, 90 mL of ODE, and 30 mL of OA in a 250 mL three-neck flask. The mixture was degassed at 120 °C for 1 h. In an argon environment, the temperature was raised to 300 °C until the solution became transparent. Then the heating mantle was removed, and the solution was allowed to cool to RT.

Synthesis of Blue- and Green-Emitting CdSe/$Cd_{1-x}Zn_xSe_{1-y}S_y$/ZnS QDs. Twenty milliliters of the Cd-oleate and Zn-oleate precursor solution (described above) was added to a 100 mL three-neck flask. The solution was degassed at 120 °C for 1 h. In an argon environment, the temperature was increased to 240 °C. At 240 °C, 0.4 μmol of CdSe QDs in toluene was quickly injected followed by an immediate but dropwise addition of a shell precursor solution (15.8 mg of Se + 256 mg of S in 4 mL of TOP) forming CdSe/$Cd_{1-x}Zn_xSe_{1-y}S_y$ QDs. To further passivate CdSe/$Cd_{1-x}Zn_xSe_{1-y}S_y$ QDs with a ZnS shell, 2 mL of 0.5 M S/TOP was added. After 90 min, the heating mantle was removed, and the solution was allowed to cool to RT. At around 60 °C, 10 mL of hexane was added. The final CdSe/$Cd_{1-x}Zn_xSe_{1-y}S_y$/ZnS QDs were precipitated with acetone twice and then redispersed in the desired solvent.

Synthesis of Red-Emitting CdSe/$Cd_{1-x}Zn_xSe_{1-y}S_y$/ZnS QDs. For synthesis of cadmium-based QDs with graded architecture, we have adopted and modified a previously reported method.[21,34] We placed 1 mmol of CdO, 2 mmol of $Zn(Ac)_2$, 5 mL of oleic acid, and 15 mL of octadecene were placed in a three-neck flask. The mixture was then degassed for 1 h at 150 °C followed by a temperature increase to 300 °C. After the solution became transparent, 0.4 mL of 1 M Se/TOP was quickly injected. To passivate the QD surface, 0.3 mL of dodecanethiol was added dropwise. Then, to fully passivate the QD with a thick shell, 1 mL of 2 M S/TOP was added and allowed to react for several minutes. After the solution was cooled, 10 mL of hexane was added.

Synthesis of PbSe/$PbSe_{1-y}S_y$/PbS IR QDs. For cation exchange of cadmium-based QDs into lead-based QDs, we adopted and modified a previously reported method.[12] To a three-neck flask was added 5 mL of oleylamine and 1 mmol (278 mg) of $PbCl_2$. The solution was degassed at RT for 1 h. The temperature was raised to 190 °C in an argon environment. One milliliter of 0.05 M CdSe/$Cd_{1-x}Zn_xSe_{1-y}S_y$/ZnS QDs in ODE was quickly injected and allowed to undergo cation exchange for desired reaction times. The heating mantle was then removed and allowed to cool to RT. At around 70 °C, 4 mL of OA and 5 mL of hexane were added to the solution. The PbSe/$PbSe_{1-y}S_y$/PbS QDs were precipitated with methanol twice and dispersed in hexane. The final hexane solution was centrifuged at 1000 rpm (unreacted $PbCl_2$ precipitates), and the supernatant was collected for further characterization.

Fabrication of IR QD LEDs. To fabricate IR-emitting LEDs, the PbSe/$PbSe_{1-y}S_y$/PbS IR QDs were mixed with poly(methyl methacrylate) in toluene to create a viscous polymer solution. The QD/polymer solution was then dropcast onto a blue chip LED and allowed to dry. The blue chip was then illuminated, and the IR emission spectra of the QD down-converted LED were recorded.

Characterization. The morphology of as-prepared CdSe QDs, CdSe/$Cd_{1-x}Zn_xSe_{1-y}S_y$/ZnS QDs, and PbSe/$PbSe_{1-x}S_x$/PbS QDs was examined by using a JEOL 100CX II TEM. High-resolution TEM images as well as EDS (point scan) measurements were obtained by an FEI Tecnai G2 F30 TEM. EDS (area scan) was performed by a LEO 1530 SEM. The X-ray diffraction (XRD) patterns were obtained by using a PANalytical Empyrean Alpha-1 X-ray diffractometer. Absorption and emission spectra up to NIR wavelengths were recorded by using a UV−vis spectrometer (UV-2600, Shimadzu) and a spectrofluorophotometer (RF-5301PC, Shimadzu), respectively. For IR absorption spectra, a Cary 5000 UV−vis−NIR spectrophotometer which is capable to measure absorbance up to 3300 nm was utilized. For IR PL spectra, a FieldSpec 3 spectroradiometer was utilized.

The PLQY (η) of the diluted QD in TCE solution samples were measured similarly as reported in the literature[29] on the following equation:

https://dx.doi.org/10.1021/acsanm.0c02434
ACS Appl. Nano Mater. 2020, 3, 11335−11343

$$\eta = \eta_r \frac{FA_r n^2 \lambda}{F_r A n_r^2 \lambda_r} \quad (1)$$

where F is the integrated emission intensity, A is the absorption rate at the excitation wavelength of 800 nm, n is the refractive index of the solvent, and λ is the peak emission wavelength. The subscript "r" represents the IR-1048 dye (Sigma-Aldrich) as the reference for PLQY measurements. The PLQY of the IR-1048 dye in diluted ethanol solution is reported to be 0.1%, with a peak emission at 1048 nm.[31] Both the QD samples and the dye were excited with a 0.8 W laser diode emitting at 800 nm, and the fluorescence spectra were recorded with the radiance calibrated FieldSpec 3 spectroradiometer.

■ ASSOCIATED CONTENT

Supporting Information

The Supporting Information is available free of charge at https://pubs.acs.org/doi/10.1021/acsanm.0c02434.

Additional optical and structural characterization data including PL, absorption, XRD, EDS, TEM, STEM, XPS, and so on to support the conclusions of this paper (PDF)

■ AUTHOR INFORMATION

Corresponding Authors

Zhitao Kang − *School of Materials Science and Engineering and Georgia Tech Research Institute, Georgia Institute of Technology, Atlanta, Georgia 30332, United States;* orcid.org/0000-0001-6736-7809; Email: zhitao.kang@gtri.gatech.edu

Zhiqun Lin − *School of Materials Science and Engineering, Georgia Institute of Technology, Atlanta, Georgia 30332, United States;* orcid.org/0000-0003-3158-9340; Email: zhiqun.lin@mse.gatech.edu

Authors

Young Jun Yoon − *School of Materials Science and Engineering, Georgia Institute of Technology, Atlanta, Georgia 30332, United States*

Gill Biesold − *School of Materials Science and Engineering, Georgia Institute of Technology, Atlanta, Georgia 30332, United States*

Shuang Liang − *School of Materials Science and Engineering, Georgia Institute of Technology, Atlanta, Georgia 30332, United States*

Zewei Wang − *School of Materials Science and Engineering, Georgia Institute of Technology, Atlanta, Georgia 30332, United States*

Yeu Wei Harn − *School of Materials Science and Engineering, Georgia Institute of Technology, Atlanta, Georgia 30332, United States*

Cheng-Hsin Lu − *School of Materials Science and Engineering, Georgia Institute of Technology, Atlanta, Georgia 30332, United States*

Richard Kim − *School of Materials Science and Engineering and Georgia Tech Research Institute, Georgia Institute of Technology, Atlanta, Georgia 30332, United States*

Wendy Yao − *Georgia Tech Research Institute, Georgia Institute of Technology, Atlanta, Georgia 30332, United States*

Sarah Lane − *Georgia Tech Research Institute, Georgia Institute of Technology, Atlanta, Georgia 30332, United States*

J. Christopher James − *Georgia Tech Research Institute, Georgia Institute of Technology, Atlanta, Georgia 30332, United States*

Yong Ding − *School of Materials Science and Engineering, Georgia Institute of Technology, Atlanta, Georgia 30332, United States*

Complete contact information is available at: https://pubs.acs.org/10.1021/acsanm.0c02434

Author Contributions

Y.J.Y. and G.B. contributed equally to this work.

Notes

The authors declare no competing financial interest.

■ ACKNOWLEDGMENTS

This work was partly supported by DOD/Army STTR project (No. W56KGU-17-C-0053) and NSF projects (ECCS 1914562 and CMMI 1914713).

■ REFERENCES

(1) Kershaw, S. V.; Susha, A. S.; Rogach, A. L. Narrow Bandgap Colloidal Metal Chalcogenide Quantum Dots: Synthetic Methods, Heterostructures, Assemblies, Electronic and Infrared Optical Properties. *Chem. Soc. Rev.* **2013**, *42* (7), 3033−3087.

(2) Mishra, N.; Mukherjee, B.; Xing, G.; Chakrabortty, S.; Guchhait, A.; Lim, J. Y. Cation Exchange Synthesis of Uniform PbSe/PbS Core/Shell Tetra-pods and Their Use as Near-Infrared Photodetectors. *Nanoscale* **2016**, *8* (29), 14203−14212.

(3) Li, S.; Bian, K.; Zhou, X.; Lu, P.; Liu, S.; Brener, I.; Sinclair, M.; Luk, T.; Schunk, H.; Alarid, L.; Clem, P. G.; Wang, Z.; Fan, H. Pressure Compression of CdSe Nanoparticles into Luminescent Nanowires. *Sci. Adv.* **2017**, *3* (5), No. e1602916.

(4) Bai, F.; Bian, K.; Huang, X.; Wang, Z.; Fan, H. Pressure Induced Nanoparticle Phase Behavior, Property, and Applications. *Chem. Rev.* **2019**, *119* (12), 7673−7717.

(5) Liu, T. C. Y. *Semiconductor Nanocrystals and Metal Nanoparticles: Physical Properties and Device Applications*; CRC Press: 2016.

(6) Dalven, R. A Review of the Semiconductor Properties of PbTe, PbSe, PbS and PbO. *Infrared Phys.* **1969**, *9* (4), 141−184.

(7) McGuire, J. A.; Sykora, M.; Joo, J.; Pietryga, J. M.; Klimov, V. I. Apparent Versus True Carrier Multiplication Yields in Semiconductor Nanocrystals. *Nano Lett.* **2010**, *10* (6), 2049−2057.

(8) Beard, M. C.; Midgett, A. G.; Hanna, M. C.; Luther, J. M.; Hughes, B. K.; Nozik, A. J. Comparing Multiple Exciton Generation in Quantum Dots To Impact Ionization in Bulk Semiconductors: Implications for Enhancement of Solar Energy Conversion. *Nano Lett.* **2010**, *10* (8), 3019−3027.

(9) Wise, F. W. Lead Salt Quantum Dots: the Limit of Strong Quantum Confinement. *Acc. Chem. Res.* **2000**, *33* (11), 773−780.

(10) Pietryga, J. M.; Schaller, R. D.; Werder, D.; Stewart, M. H.; Klimov, V. I.; Hollingsworth, J. A. Pushing the Band Gap Envelope: Mid-Infrared Emitting Colloidal PbSe Quantum Dots. *J. Am. Chem. Soc.* **2004**, *126* (38), 11752−11753.

(11) Pietryga, J. M.; Werder, D. J.; Williams, D. J.; Casson, J. L.; Schaller, R. D.; Klimov, V. I.; Hollingsworth, J. A. Utilizing the Lability of Lead Selenide to Produce Heterostructured Nanocrystals with Bright, Stable Infrared Emission. *J. Am. Chem. Soc.* **2008**, *130* (14), 4879−4885.

(12) Zhang, J.; Gao, J.; Church, C. P.; Miller, E. M.; Luther, J. M.; Klimov, V. I.; Beard, M. C. PbSe Quantum Dot Solar Cells with More than 6% Efficiency Fabricated in Ambient Atmosphere. *Nano Lett.* **2014**, *14* (10), 6010−6015.

(13) Talapin, D. V.; Murray, C. B. PbSe Nanocrystal Solids for n- and p-Channel Thin Film Field-Effect Transistors. *Science* **2005**, *310* (5745), 86−89.

(14) Luther, J. M.; Law, M.; Song, Q.; Perkins, C. L.; Beard, M. C.; Nozik, A. J. Structural, Optical, and Electrical Properties of Self-Assembled Films of PbSe Nanocrystals Treated with 1,2-Ethanedithiol. *ACS Nano* **2008**, *2* (2), 271−280.
(15) Sykora, M.; Koposov, A. Y.; McGuire, J. A.; Schulze, R. K.; Tretiak, O.; Pietryga, J. M.; Klimov, V. I. Effect of Air Exposure on Surface Properties, Electronic Structure, and Carrier Relaxation in PbSe Nanocrystals. *ACS Nano* **2010**, *4* (4), 2021−2034.
(16) Yanover, D.; Vaxenburg, R.; Tilchin, J.; Rubin-Brusilovski, A.; Zaiats, G.; Čapek, R. K.; Sashchiuk, A.; Lifshitz, E. Significance of Small-Sized PbSe/PbS Core/Shell Colloidal Quantum Dots for Optoelectronic Applications. *J. Phys. Chem. C* **2014**, *118* (30), 17001−17009.
(17) Kim, S.; Marshall, A. R.; Kroupa, D. M.; Miller, E. M.; Luther, J. M.; Jeong, S.; Beard, M. C. Air-Stable and Efficient PbSe Quantum-Dot Solar Cells Based upon ZnSe to PbSe Cation-Exchanged Quantum Dots. *ACS Nano* **2015**, *9* (8), 8157−8164.
(18) Zhang, J.; Chernomordik, B. D.; Crisp, R. W.; Kroupa, D. M.; Luther, J. M.; Miller, E. M.; Gao, J.; Beard, M. C. Preparation of Cd/Pb Chalcogenide Heterostructured Janus Particles via Controllable Cation Exchange. *ACS Nano* **2015**, *9* (7), 7151−7163.
(19) Wei, S.-H.; Zunger, A. Electronic and structural anomalies in lead chalcogenides. *Phys. Rev. B: Condens. Matter Mater. Phys.* **1997**, *55* (20), 13605−13610.
(20) Lifshitz, E.; Brumer, M.; Kigel, A.; Sashchiuk, A.; Bashouti, M.; Sirota, M.; Galun, E.; Burshtein, Z.; Le Quang, A. Q.; Ledoux-Rak, I.; Zyss, J. Air-Stable PbSe/PbS and PbSe/$PbSe_xS_{1-x}$ Core-Shell Nanocrystal Quantum Dots and Their Applications. *J. Phys. Chem. B* **2006**, *110* (50), 25356−25365.
(21) Jung, J.; Lin, C. H.; Yoon, Y. J.; Malak, S. T.; Zhai, Y.; Thomas, E. L.; Vardeny, V.; Tsukruk, V. V.; Lin, Z. Crafting Core/Graded Shell-Shell Quantum Dots with Suppressed Re-Absorption and Tunable Stokes Shift as High Optical Gain Materials. *Angew. Chem., Int. Ed.* **2016**, *55* (16), 5071−5075.
(22) Rubin-Brusilovski, A.; Jang, Y.; Shapiro, A.; Safran, A.; Sashchiuk, A.; Lifshitz, E. Influence of Interfacial Strain on Optical Properties of PbSe/PbS Colloidal Quantum Dots. *Chem. Mater.* **2016**, *28* (24), 9056−9063.
(23) Yu, W. W.; Qu, L.; Guo, W.; Peng, X. Experimental Determination of the Extinction Coefficient of CdTe, CdSe, and CdS Nanocrystals. *Chem. Mater.* **2003**, *15* (14), 2854−2860.
(24) Dabbousi, B. O.; Rodriguez-Viejo, J.; Mikulec, F. V.; Heine, J. R.; Mattoussi, H.; Ober, R.; Jensen, K. F.; Bawendi, M. G. CdSe)ZnS Core-Shell Quantum Dots: Synthesis and Characterization of a Size Series of Highly Luminescent Nanocrystallites. *J. Phys. Chem. B* **1997**, *101* (46), 9463−9475.
(25) Beberwyck, B. J.; Surendranath, Y.; Alivisatos, A. P. Cation Exchange: A Versatile Tool for Nanomaterials Synthesis. *J. Phys. Chem. C* **2013**, *117* (39), 19759−19770.
(26) Luther, J. M.; Zheng, H.; Sadtler, B.; Alivisatos, A. P. Synthesis of PbS Nanorods and Other Ionic Nanocrystals of Complex Morphology by Sequential Cation Exchange Reactions. *J. Am. Chem. Soc.* **2009**, *131* (46), 16851−16857.
(27) Brumer, M.; Kigel, A.; Amirav, L.; Sashchiuk, A.; Solomesch, O.; Tessler, N.; Lifshitz, E. PbSe/PbS and PbSe/$PbSe_xS_{1-x}$ Core/Shell Nanocrystals. *Adv. Funct. Mater.* **2005**, *15* (7), 1111−1116.
(28) Mokari, T.; Habas, S. E.; Zhang, M.; Yang, P. Synthesis of Lead Chalcogenide Alloy and Core-Shell Nanowires. *Angew. Chem., Int. Ed.* **2008**, *47* (30), 5605−5608.
(29) Bakueva, L.; Gorelikov, I.; Musikhin, S.; Zhao, X. S.; Sargent, E. H.; Kumacheva, E. PbS Quantum Dots with Stable Efficient Luminescence in the Near-IR Spectral Range. *Adv. Mater.* **2004**, *16* (11), 926−929.
(30) Weidman, M. C.; Beck, M. E.; Hoffman, R. S.; Prins, F.; Tisdale, W. A. Monodisperse, Air-Stable PbS Nanocrystals via Precursor Stoichiometry Control. *ACS Nano* **2014**, *8* (6), 6363−6371.
(31) Casalboni, M.; De Matteis, F.; Prosposito, P.; Quatela, F.; Sarcinelli, F. Fluorescence Efficiency of Four Infrared Polymethine Dyes. *Chem. Phys. Lett.* **2003**, *373* (3), 372−378.
(32) Shao, Q.; Ding, H.; Yao, L.; Xu, J.; Liang, C.; Jiang, J. Photoluminescence Properties of a $ScBO_3$:Cr_{3+} Phosphor and its Applications for Broadband Near-Infrared LEDs. *RSC Adv.* **2018**, *8* (22), 12035−12042.
(33) Son, D. H.; Hughes, S. M.; Yin, Y.; Paul Alivisatos, A. Cation Exchange Reactions in Ionic Nanocrystals. *Science* **2004**, *306* (5698), 1009−1012.
(34) Bae, W. K.; Char, K.; Hur, H.; Lee, S. Single-Step Synthesis of Quantum Dots with Chemical Composition Gradients. *Chem. Mater.* **2008**, *20* (2), 531−539.

https://dx.doi.org/10.1021/acsanm.0c02434
ACS Appl. Nano Mater. 2020, 3, 11335−11343